Integrated Numerical Modeling to Quantify Transport and Fate of Microplastics in the Hyporheic Zone

---

Authors

Franz Dichgans[1*], Jan-Pascal Boos[2], Pouyan Ahmadi[1], Sven Frei[2], Jan H. Fleckenstein[1,3]

[1] Helmholtz Centre for Environmental Research - UFZ, Department Hydrogeology, Permoserstr. 15, 04318 Leipzig, Germany

[2] Department of Hydrology, Bayreuth Center of Ecology and Environmental Research (BayCEER), University of Bayreuth, 95440 Bayreuth, Germany

[3] Hydrologic Modeling Unit, Bayreuth Center of Ecology and Environmental Research (BayCEER), University of Bayreuth, 95440 Bayreuth, Germany

* Corresponding author at Helmholtz Centre for Environmental Research - UFZ, Department Hydrogeology, Permoserstr. 15, 04318 Leipzig, Germany. Email-address: franz.dichgans@ufz.de

---

Abstract

Despite the significance of rivers and streams as pathways for microplastics (MP) entering the marine environment, limited research has been conducted on the behavior of MP within fluvial systems. Specifically, there is a lack of understanding regarding the infiltration and transport dynamics of MP across the streambed interface and within the hyporheic sediments. In this study, transport and retention of MP are investigated using a new numerical modeling approach. The model is built as a digital twin of accompanying flume experiments, which are used to validate the simulation results. The model accurately represents particle transport in turbulent water flow and within the hyporheic zone (HZ). Simulations for transport and infiltration of 1 µm MP particles into a sandy streambed demonstrate that the advection-dispersion equation can be used to adequately represent particle transport for pore-scale sized MP within the HZ. To assess the applicability of the modeling framework for larger MP, the experiment was repeated using 10 µm particles. The larger particles exhibited delayed infiltration and transport behavior, and while the model successfully represented the spatial extent of particle transport through the HZ, it was unable to fully replicate hyporheic transit times. This study is the first to combine explicit validation against experimental data, encompassing qualitative observations of MP concentration patterns and quantification of fluxes. By that, it significantly contributes to our understanding of MP transport processes in fluvial systems. The study also highlights the advantages and limitations of employing a fully integrated modeling approach to investigate the transport and retention behavior of MP in rivers and streams.

Keywords

microplastics, hyporheic zone, hyporheic exchange, computational fluid dynamics (CFD), OpenFOAM

1 INTRODUCTION

In recent years, microplastics (MP) have been identified as a global environmental micropollutant (Andrady, 2011; Napper and Thompson, 2020). Since the term was coined by marine researchers (Thompson et al., 2004), research has long been focusing on marine environments (D'Avignon et al., 2022). MP are synthetic particles with a size range from 1 µm to 5 mm (Frias and Nash, 2019). The widespread use of plastic products has also led to an increase in plastic pollution. Abrasion during use as well as improper disposal leads to fragmentation of larger plastic debris into smaller particles that ubiquitously can be found in the environment (Horton and Dixon, 2018; Koelmans et al., 2014; Petersen and Hubbart, 2021; Ahmadi et al., 2022). As the vast majority of polymers released into the environment are not biodegradable, MP pollution is a long-lasting problem (Laforsch et al., 2021). The effects of MP pollution on aquatic organisms (pelagic, benthic and hyporheic), specifically under environmental conditions are still largely unknown and subject of current research (Besseling et al., 2017a; Burns and Boxall, 2018; Windsor et al., 2019), though initial works indicate adverse effects (Choi et al., 2021; Laforsch et al., 2021).

Pollutants, including MP, are transported from terrestrial sources via rivers and streams into marine environments. As a major transport pathway, streams and rivers play a key role in understanding the fate of MP in the environment (Mani et al., 2016; Meijer et al., 2021; Schmidt et al., 2017). Rivers are not only transport corridors, but also retain considerable amounts of MP in their sediments (Castañeda et al., 2014; Constant et al., 2021; Frei et al., 2019; Laermanns et al., 2021; Mani et al., 2019; Nizzetto et al., 2016). However, most studies on MP transport in fluvial systems have mainly focused on identifying dominant transport pathways from source areas to marine systems, neglecting the impact of MP pollution on the riverine environment and small-scale transport phenomena. These coarser-scaled approaches, frequently rely on often not well tested analogies from sediment transport in fluvial environments (Besseling et al., 2017b; Lebreton et al., 2017; Nizzetto et al., 2016; Siegfried et al., 2017) or are simplifying the mechanistic processes in riverine environments (Domercq et al., 2022; Drummond et al., 2022, 2020). First laboratory studies with MP particles of approximately neutral buoyancy suggest that these particles are conservatively transported in the surface flow similar to solutes (Cook et al., 2020; Stride et al., 2023).

The hyporheic zone (HZ), occupying the uppermost sediment layers in a river and the interface between the river and its adjoining aquifer is provider of many ecosystem services (Lewandowski et al., 2019). It can be defined as comprising saturated streambed sediments with flow paths originating from and subsequently returning to the surface water (Harvey and Bencala, 1993; Lewandowski et al., 2019)Studies have shown high abundances of different MP particles in the HZ without specifically investigating the associated transport and retention mechanisms leading to the observed accumulation (Frei et al., 2019). However, a mechanistic understanding of processes resulting in the accumulation of MP in streambed sediments is essential for understanding the impact of MP in the HZ.

The effects of pollutants on organisms are strongly linked to the exposure time (Amoatey and Baawain,

2019), which is in turn correlated with the transport time scales. Besides hazardous effects after ingestion (von Moos et al., 2012), MP particles also can leach potentially harmful substances (Schrank et al., 2019) and are known as vectors for pathogens (Kirstein et al., 2016; McCormick et al., 2014), further highlighting the importance to estimate hyporheic transit times for MP. Transfer of MP from surface flow into the hyporheic sediments and mobility within porous media needs to be studied to accurately predict hyporheic transit times and retention quantities in fluvial systems (Drummond et al., 2020). The retention of MP in stream networks in turn affects the transfer of MP from the terrestrial to the marine system (Besseling et al., 2017b) and hence controls MP loadings to the sea. Laboratory studies have been performed to specifically investigate the hydrodynamic controls on MP transport processes relevant to fluvial systems, but results from these studies have not been extrapolated to larger scales (Hoellein et al., 2019; Waldschläger and Schüttrumpf, 2020). This gap can be closed through calibrated hydro-numerical models, which allow extrapolation of small-scale findings to larger scales such as river reaches or entire catchments.

Process based modeling of surface-groundwater interactions as well as hyporheic exchange is often carried out using weakly (sequentially) coupled models: Here, the river hydrodynamics are simulated without accounting for advective exchange of water with the HZ and where the pressure distribution along the streambed interface is used as a boundary condition for a separate HZ model (Dudunake et al., 2020; Ren and Zhao, 2020; Trauth et al., 2013; Xiao et al., 2022). Other studies have focused on conservative and reactive solute transport and the resulting concentration patterns in the HZ in fully-coupled versus weakly-coupled models (Li et al., 2020). It has been suggested to use integral modeling for a detailed analysis of hyporheic exchange processes, which can improve the accuracy of simulation results (Broecker et al., 2019). These integrated approaches have been used mostly for the validated investigation of solute transport in streambeds and were a significant advance in the modeling of hyporheic exchange processes (Broecker et al., 2019, 2018; Sobhi Gollo et al., 2021, 2022a, 2022b). These works mostly focused on solute transport and not on particle transport and were focused more on capturing the overall spatiotemporal distribution of a dye tracer in the hyporheic sediments, while locally occurring concentrations could not be fully validated due to the lack of a respective dataset.

In this paper we address this gap and present a novel numerical modeling scheme based on the OpenFOAM toolbox, which allows an integrated hydrodynamic simulation of the interactions between the surface water and the HZ. The numerical modeling is based on data from laboratory flume experiments where a novel tracking method was used to investigate and quantify the transfer of MP between surface flow and streambed sediments (Boos et al., 2021). By building a digital twin model of the laboratory setup, the results of the numerical model can be directly validated. This specific combination of integrated modeling and a reference flume experiment with a full quantification of MP transport in the open water and in the hyporheic sediments enables us to investigate the following research questions on MP transport in fluvial systems with unprecedented rigor:

- Can the proposed integrated mechanistic CFD methodology adequately reproduce the transport behavior of very small MP particles, as investigated in the accompanying laboratory experiments qualitatively as well as quantitatively?
- Are sufficiently small MP particles transported in the HZ in a similar manner as a conservative solute tracer?
- How does particle behavior in the flume and HZ change with increasing particle size?
- Can commonly-used concepts to simulate solute transport in porous media be adapted to account for deviating behavior of larger particles?

2 METHODOLOGY

2.1 Model Overview

To investigate the transport mechanisms for MP particles at the streambed interface, a two-fold approach has been developed. A numerical model was set up using the open-source C++ suite of computational fluid dynamics (CFD) solvers OpenFOAM (Weller et al., 1998). The model was set up as a digital twin of accompanying laboratory experiments. In the experiments MP transport was tracked in a flume and across a model streambed interface using novel optical methods (Boos et al., 2021). The experimental results were used to validate the numerical model.

2.2 Case Description

The flume experiments (Figure 1) were performed using sand (with a median grain size d_{50} = 1.04 mm and a hydraulic conductivity range of $k_s = 3.44^{-4}$ m/s) to mimic naturally occurring streambeds (Haque and Mahmood, 1985). Prior to each experiment, the sand was carefully sculpted into rippled bedforms, adhering to geometrical properties representative for natural bedforms. The flume was inclined by 0.003 m/m and operated with deionized water at a constant discharge of 0.27 L/s.

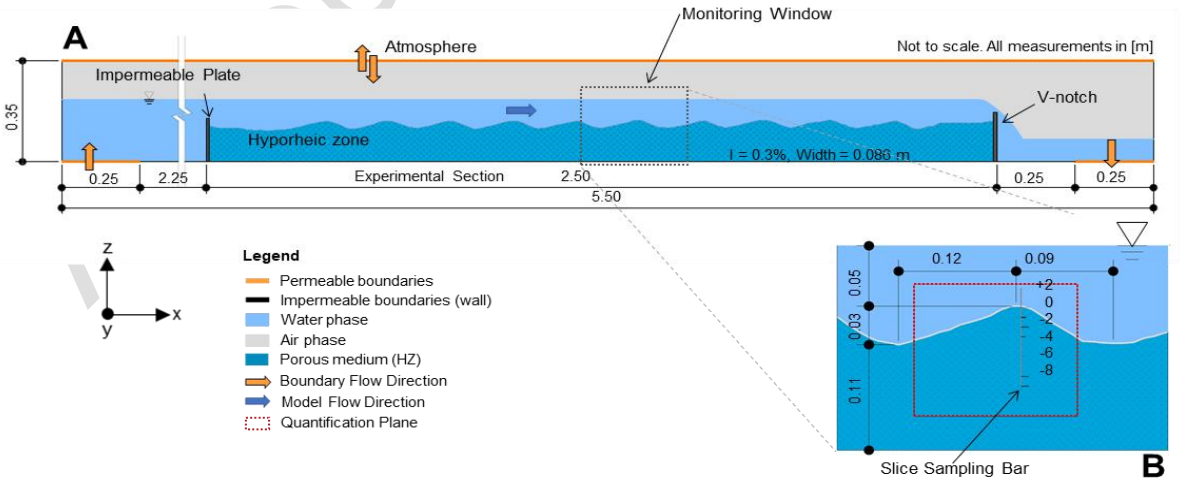

Figure 1. Model setup: (A) Longitudinal section of the model setup and monitoring locations, , (B) Detailed view of the monitoring window.

Sediments were stabilized by using plates at the up- and downstream sides of the flume (Figure 1A). A V-notch weir located at the downstream plate was used for the quantification of flume discharge. The experiments were carried out using fluorescent 1 µm and 10 µm polystyrene (PS, density 1050 kg/m³) microbeads.

Prior to the MP application, deionized water was pumped through the flume and recirculated for 120 min until a quasi-steady state (a condition where bedforms were stable and surface water flow was perceived as quasi steady and uniform based on optical inspection) was reached. After opening the water circuit, the MP sample was injected at the inlet of the flume in a single pulse and the MP propagation in the flume was monitored for a total duration of 2,000 s. During the MP experiments the flume was operated in a non-recirculating setup to allow for an accurate monitoring of the entire MP breakthrough without re-feeding the particles back into the flume.

The experimental methods which were used in the experiments carried out for this work are described in detail in (Boos et al., 2021). The MP concentration in the streambed sediments was continuously measured for a monitoring window (Figure 1B) using a Fluorescence-Imaging-System (FIS) through the glass sidewall of the flume (Figure 2). Fluorometers continuously monitored the MP concentrations in the surface water at the up- and downstream ends of the experimental section. The setup was supplemented with a 2D laser profiler to digitize the bedform geometry and continuously monitor a representative subset of the bedform during the experiments to ensure bedform stability.

The water level was monitored continuously at six locations along the flume centerline with ultrasonic water level sensors, mounted on top of the flume. 2D surface flow velocities in the flume (Figure 1A) were measured using Particle-Image-Velocimetry (PIV) (Boos et al., 2022). The velocity field was acquired at three adjoining ripples in the monitoring window to validate the numerical model.

Table 1. Monitoring setup for the laboratory flume.

#	Parameter	Instrument	Monitoring Location
1	Water Surface Elevation	Ultrasonic sensors	Six point measurements along the experimental section/control volume
2	Discharge	Electromagnetic flow meter + v-Notch	Feeder pipe / Downstream end
3	Bedform Geometry	2D X-Z laser profiler	Complete bedform
4	2D (X-Z) velocity field	Particle-Image-Velocimetry (PIV)	Reference monitoring window
5	MP concentration in surface water	Fluorometer	Inlet and outlet of the experimental section
6	MP concentration in surface water and HZ	Fluorescence-Imaging-System (FIS)	Reference monitoring window
7	Temperature	Levelogger	Inlet Tank

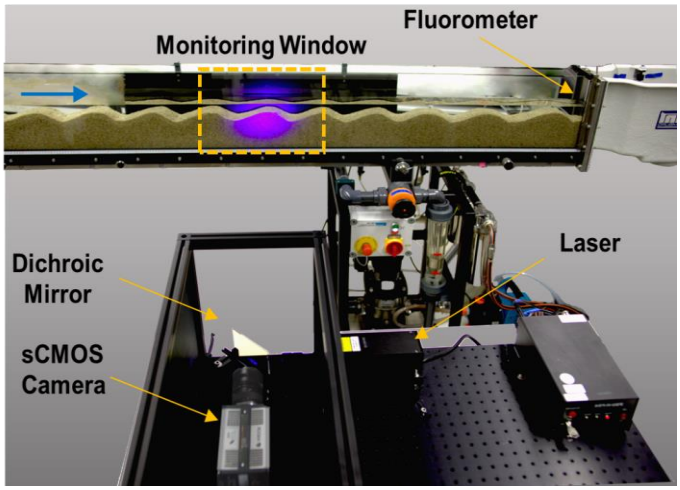

Figure 2. MP monitoring setup in the hydraulic laboratory.

2.3 Turbulent Flow and Transport Modeling

2.3.1 Governing Equations

To model microplastic transport in the open water (stream) and in the sediments (HZ), an integrated hydrodynamic model has been set up using the numerical toolbox OpenFOAM (version v2112). The model is solved using InterFoam, a solver for the computation of two-phase flows with immiscible, isothermal, and incompressible fluids. It solves the three-dimensional Navier-Stokes equations based on the finite volume method. The phase interface is tracked using the volume of fluid (VoF) method (Hirt and Nichols, 1981).

The HZ has been defined as a porous continuum with the hydraulic losses being calculated based on the Darcy-Forchheimer equation (Equation 1). The computed losses are applied to the momentum equation as a sink term S:

$$S = -\left(\mu D + \frac{\rho|U|}{2}F\right)U \tag{1}$$

Where μ is the dynamic viscosity of the fluid [kg/m/s], ρ the density of the fluid [kg/m³], D the Darcy coefficient [1/m²], F the Forchheimer coefficient [1/m] and U the flow velocity vector [m/s]. The Darcy coefficient D accounts for the viscous flow losses in the porous medium. In the present case, it is set to $D = 4.995\ 10^{-7}$ 1/m², based on the laboratory analysis of the utilized bedform material as well as validation runs with the numerical model. The Forchheimer coefficient F accounts for the inertial losses within the porous medium, which are relevant in turbulent flow regimes. In the investigated case, the porous flow regime within the HZ is generally laminar with Reynolds numbers < 10, with only singular areas within the first 2 cm below the bed surface on the upstream ripple crest being located in the lower region of the transitional regime with Reynolds numbers < 50 (Dybbs and Edwards, 1984). Therefore, the coefficient is

set to F = 0.

Transport of MP particles is simulated using the scalarTransport function object, which solves the advection-dispersion (ADE) equation for the non-reactive transport of a conservative solute at the end of each time step. The use of the ADE to simulate the transport of 1 µm MP particles in the hyporheic sediments was motivated by recent evidence that MP particles in this size range show transport behavior in groundwater similar to that of conservative solutes (Goeppert and Goldscheider, 2021). To be able to account for possible particle retention and remobilization in the pore space due to a variety of processes, such as physical clogging and heteroaggregation, a dimensionless advective retardation factor *R* has been added to the scalar transport equation function object, resulting in the following transport equation:

$$\frac{\partial}{\partial t}(C) + \frac{1}{R}\nabla \cdot (uC) - \nabla \cdot (D_T \nabla C) = S_C \quad (2)$$

where *C* represents the scalar, *U* the flow velocity vector [m/s], D_C the dispersivity of the scalar [m²/s], *R* the dimensionless retardation factor and S_C the source term. In accordance with our own observations and the findings of (Broecker et al., 2021), the scalar dispersivity is set to $D_C = 2\times10^{-9}$ m²/s, accounting for the molecular diffusivity only. By considering the particle cloud as a conservative scalar tracer, the transport processes at the subgrid scale such as particle collision, homo- or heteroaggregation processes are not explicitly resolved. Furthermore, this assumes a largely uniform distribution of particles in the particle cloud. Possible influences of the particle on the surrounding flow field are not considered as well.

In natural flow over streambed ripples, complex turbulent structures can evolve at the lee side of each ripple, which can either be directly modeled numerically with a very fine mesh or indirectly approximated with a turbulence model (Janssen et al., 2012). For the present case, a large eddy simulation (LES) model was utilized to resolve turbulent patterns. This model separates smaller turbulent structures and approximates them algebraically, while larger eddies are directly solved (Ferziger et al., 2020). For the representation of the subgrid-scale, the Smagorinsky subgrid-scale model was used.

Different commonly used and computationally less expensive methods for representing turbulence patterns (such as k-ϵ or k- ω SST) were tested, but resulted in less accurate flow fields, especially regarding the representation of secondary currents as well as the flow separation and eddy zone at the lee side of each stream ripple. As these inaccuracies lead to an underestimation of the hyporheic exchange rate, these turbulence modeling schemes were not applied. This is also matching the findings of (Broecker et al., 2021; Sobhi Gollo et al., 2022b).

2.3.2 Discretization

Discretization of the model domain was done using different meshing algorithms of the OpenFOAM suite. To allow for a clear separation of the HZ from the surface flow domain, the mesh cell boundaries have to be adapted to the bedform geometry. This is achieved by using the algorithm MoveDynamicMesh, which deforms the hexahedral base mesh to given geometry constraints. The weir plates in the flume are implemented using SnappyHexMesh. The developed approach ensures that the mesh is dominated by

hexahedral and split-hexahedral mesh cells, minimizing non-orthogonality (e.g. in comparison to prismatic meshes) and allowing for an efficient and accurate representation of the geometry in the mesh. The final computational mesh consists of 912,164 cells, of which >99% are hexahedral. Refinements are implemented along the sediment-water-interface and to the upstream/downstream weir plates.

LES modeling has strict requirements for the mesh resolution at the mesh boundaries (Ferziger et al., 2020). To relax these requirements, wall functions are commonly used. Instead of resolving the viscous sublayer along the walls in the mesh, they implement the physics of the near-wall flow in empirical equations. In the presented case, functions based on Spalding's law (nutUSpaldingWallFunction) were applied to the wall boundaries.

2.3.3 Boundary and Initial Conditions

Boundary conditions for key variables of the model are listed in Table 2. The inflow is realized as a fully submerged inflow boundary. The outflow boundary is defined with a fixed water level of 0.10 m. Therefore, the digital twin model does not require dynamic boundary conditions for the phase fraction variable alpha.water and can be operated with fixedValue boundary conditions for the alpha.water variable at the inlet and outlet patches. The top of the virtual flume is modeled to allow the air phase to move freely. Along the flume walls, as well as along the weir plates at the inlet/outlet of the experimental section, noSlip conditions are applied. The MP tracer has been injected in the model through a cell zone at the location of the upstream fluorometer in the laboratory model. The injected particle concentration could therefore be prescribed from the lab-measured concentrations at this point.

Table 2. Boundary Conditions for key parameters

Boundary	**p_rgh** (Pressure)	**U** (Velocity)	**alpha.water** (Phase Fraction)
Inlet	**fixedFluxPressure** Pressure gradient set to fulfill the prescribed U boundary condition	**flowRateInletVelocity** Uniform velocity field to match the prescribed flow rate	**fixedValue** Value is fixed, in this case water only
Outlet	**fixedValue** Value is fixed to maintain an approximately constant water level over the outlet patch	**pressureInletOutletVelocity** governed by the pressure boundary condition	**fixedValue** Value is fixed, in this case water only
Atmosphere	**totalPressure** Patch pressure described by subtracting the dynamic pressure from the reference pressure	**pressureInletOutletVelocity** governed by the pressure boundary condition	**inletOutlet** Zero Gradient, no return flow
Walls	**fixedFluxPressure** Pressure gradient set to fulfill the prescribed U boundary condition	**noSlip** U=0 at the wall	**zeroGradient** Zero gradient condition

3 RESULTS

3.1 Hydrodynamic Characterization of the Flow

The surface water flow field in the monitoring section showed a typical pattern for the given bedform geometry as observed in the seminal experimental work by Elliott and Brooks (Elliott and Brooks, 1997). At the specified discharge of 0.27 L/s, the water depth ranged between approx. 0.04 m over the ripple crests to 0.07 m at the inter-ripple troughs. The water elevations showed a close match between the physical and numerical models, without significant deviations (< 1 mm).

In the upper ~ 3 cm of the surface water flow, the main flow passes over the ripple crests, with a zone of maximum velocities at and downstream of the ripple crests (Figure 3). At the lee side of each ripple, a single eddy is forming, rotating around the Y-Axis (Figure 5). The flow shows a clear separation between the eddy zone and the main flow zone as shown in Figure 3. The flow velocities in the centerline of the flume approximately range from 0.08 to 0.14 m/s in the main flow and 0 to 0.08 m/s in the eddy zone.

Simulated surface flow velocities for the monitored ripple segment in general are matching the observed ones (Figures 3, 4). Shape and magnitude of relevant features of the flow velocity field, such as the general flow direction, peak over the ripple crest, and eddy zone in the ripple valley are accurately represented in the digital twin (Figure 3). Simulated and observed velocity magnitudes for surface flow are differing by only ~0.01…0.02 m/s between the PIV and CFD results. Largest differences mostly occur within the upper flow regime, whereas the velocity magnitudes in the ripple valleys are matching closely. Towards the air-water interface, the measured flow velocities are dropping sharply, whereas the modeled velocity field does not show such a sharp drop (Figure 4).

The flow conditions in the flume can be characterized as narrow open channel flow, with an aspect ratio of flow depth to channel width of ~1.25…1.5 (Jing et al., 2019). This results in pronounced secondary currents (Nikitin et al., 2021; Yang et al., 2012), which were also represented in the CFD model and are one of the reasons for using a 3D model. The PIV data did not feature cross-sectional velocity field measurements as the laboratory setup only allowed PIV recordings in the XZ plane. Hence a direct comparison of the simulated lateral flow components (Figure 3B) with experimental data was not possible.

In the hyporheic zone, the typical hyporheic flow cells as illustrated in the seminal work by (Elliott and Brooks, 1997) develop between the ripple surfaces (Figure 5). An underflow section is forming due to the inclination of the flume. Due to slight variations of the ripple geometries, the flow patterns slightly differ for consecutive ripples, but the hyporheic flow field for the ripples is independent from each other, since local infiltration patterns did not expand over more than one bedform.

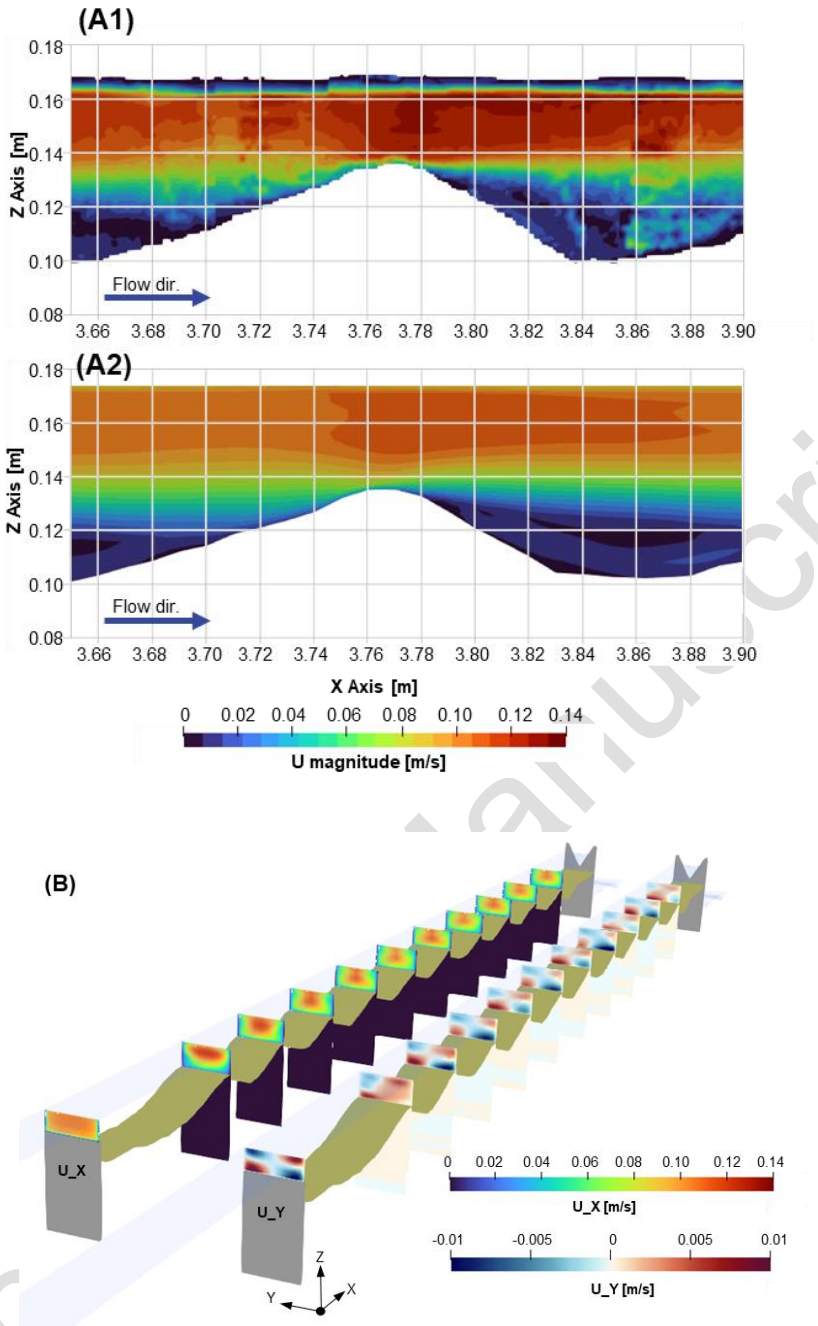

Figure 3. Velocity field in the flume: (A) Observed (A1) vs simulated (A2) velocity magnitudes in the flume centerline (B) Velocity component magnitudes in the main flow direction (U_X) and in lateral direction (U_Y) at the ripple crests, showing the friction-induced secondary currents in the narrow flume

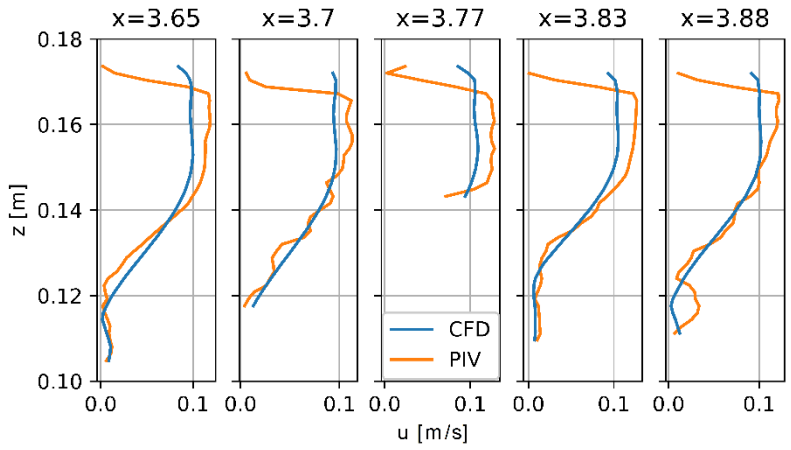

Figure 4 Comparison of measured (orange) and modeled (blue) flow velocities: Velocity profiles at select x-locations at the foot of the luv slope (x=3.65), on the luv slope (x=3.70), at the ripple crest (x=3.77), on the lee slope (x=3.83) and at the foot of the lee ripple slope (x=3.88)

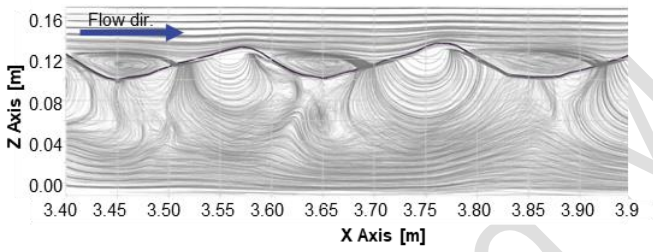

Figure 5. Flow pattern (streamlines) within the monitoring window, showing surface flow with developing eddies at the ripples' lee sides and the hyporheic flow cells with the underflow

3.2 Fully integrated simulation of open water and HZ

A key feature of this work is the integration of subsurface and surface water flow and interactions between both flow domains into a single integrated model. Calculations of the hyporheic flow conditions are based on the Navier-Stokes equations, with the energy losses through the porous medium being calculated based on the Darcy-Forchheimer equation. This allowed for an accurate representation of the hyporheic exchange processes, since hyporheic flow is not only influenced by hydrostatic pressure-differences, but also by dynamic pressure variations over the bedform resulting from the turbulent flow regime in the surface water (Broecker et al., 2019). Furthermore, the permeable streambed allowed for bidirectional exchange flows across the open-water-sediment interface, which fed back into the flow processes in the surface water. To illustrate this interrelationship, we showcase results from a simulation with an impermeable streambed in comparison to our fully integrated simulation in Figure 6. The velocity fields are distinctly different (Figure 6A1 and Figure 6A2). In particular, the shape, size, and magnitude of the eddies on the lee side of each ripple are significantly different, as backward-facing eddies are only forming when the HZ is included in the simulations. This also results in slightly different water levels in the model.

Due to these differences, the pressure field differs between a fully integrated and a quasi-non-coupled computation, as shown in Figure 6B. The plot shows the pressure difference without the hydrostatic component (p_rgh) between the cases with and without coupled HZ at the interface between surface water and HZ. As indicated by the velocity fields, the pressure differences in the ripple valleys are significant, which is caused by lack of pronounced eddy formation in the quasi non-coupled case.

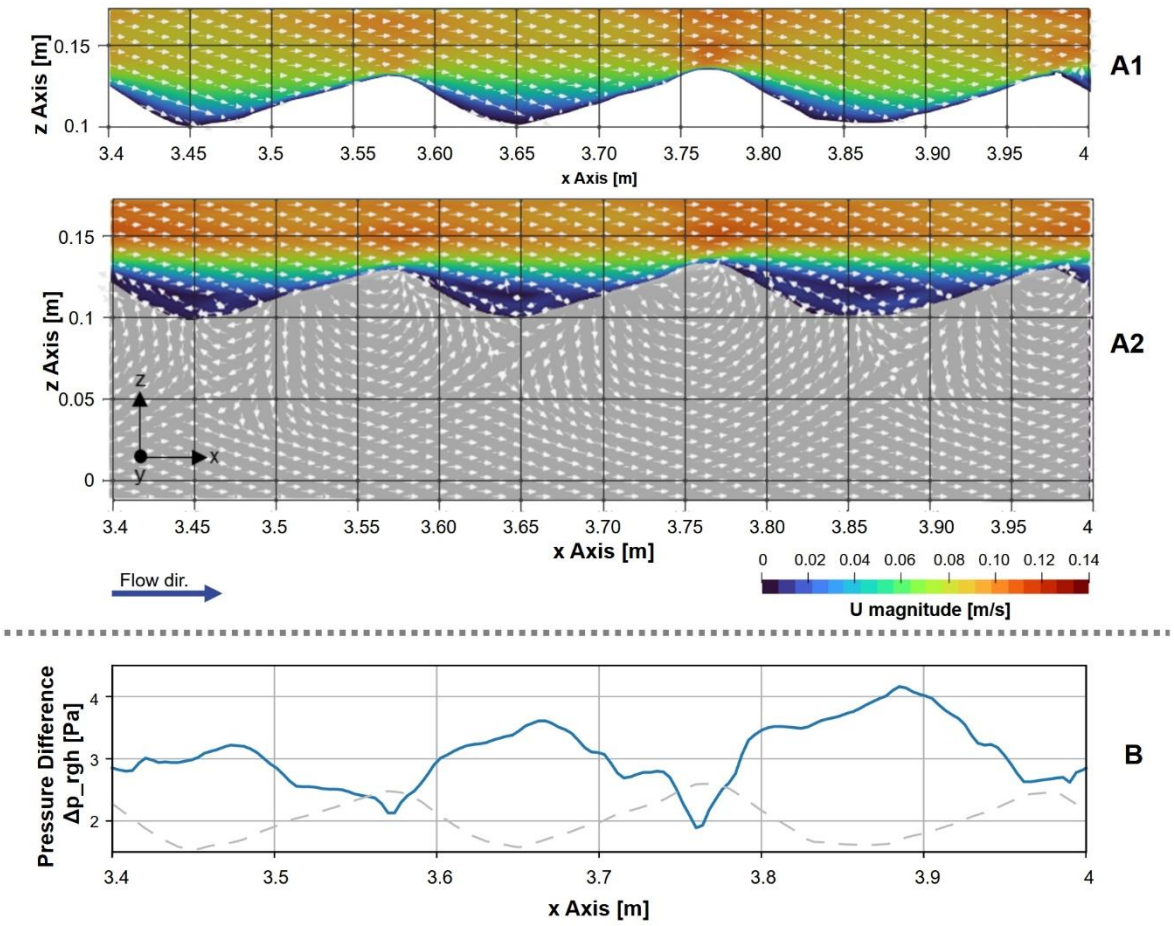

Figure 6. Velocity field in longitudinal section along the flume centerline without (A1) and with (A2) integrated modeling of a HZ. The pressure difference without the hydrostatic components (p_rgh) between the two cases is shown in (B), with the bedform shown as a dashed line.

3.3 Transport of 1 µm MP Particles

A qualitative, visual assessment of the MP infiltration into the streambed sediments showed that the complex flow patterns in the open water resulting from the narrow flume setup lead to asymmetries in particle infiltration into the HZ. These asymmetries were observed between the left and right sides of the flume, as shown also in Figure SI4. Therefore, the following comparisons between the laboratory experiment and the digital twin were carried out at the left wall of the flume, as the optical measurements of MP concentrations are taken through the left sidewall of the flume and hence reflect concentrations on that side of the flume.

The simulated and observed MP propagation through the streambed sediments in the monitoring window are compared in Figure 7. It is shown that the MP particles followed the hyporheic flow paths (Figure 5) and propagated according to the velocity field in the HZ. This led to a sickle-shaped infiltration front, which propagated through each ripple, with the majority of the MP particles exiting the ripple surface in the lower third of the lee side. Infiltration of MP took place preferentially on the upstream and downstream faces of each ripple, with an infiltration zone on the lower half of the upstream face and the main exfiltration zone on the lower third of the downstream face. Due to small variations in the ripple shapes, in- and exfiltration areas varied slightly in their location and spatial extent for each ripple sequence. Due to the flow separation between individual hyporheic flow cells (Figure 5), flow in one cell did not directly influence flows in the downstream cells. The MP front itself appeared more spatially defined in the CFD results than in the FIS dataset, specifically during the initial 800 s of the experiment.

The blanked areas visible in Figure 7 result from limitations in the optical measuring approach and inaccuracies in the conversion of the fluorescent intensity recordings to MP concentrations. In the postprocessing of the FIS data, we blanked areas where the recorded concentrations were outside of the observed local concentration range of 0…1500 mg/m³. Furthermore, around the bedform interface, implausibly large MP concentrations occur before t=500s. These are attributed to a mismatch of the calibration slopes for surface and subsurface area in the transition zone around the bedform interface and subsequently blanked as well.

The comparison of the hyporheic MP-concentration patterns between the flume experiment and the digital twin model generally shows a close match. The propagation speed of the infiltration front through the HZ as well as its shape are fairly well matched by the model as illustrated in Figure 7. In the simulations the early MP concentrations in the surface water (at 400 s in Figure 7) were slightly elevated in the ripple valleys, while the FIS recorded a more uniform MP concentration field. A comparison of the infiltration patterns in Figure 7 also suggests that the application of a retardation factor is not required to model the propagation of the 1 µm MP particles. It was therefore set to R=1 (equivalent to no retardation) for the modeling of 1 µm MP particle transport.

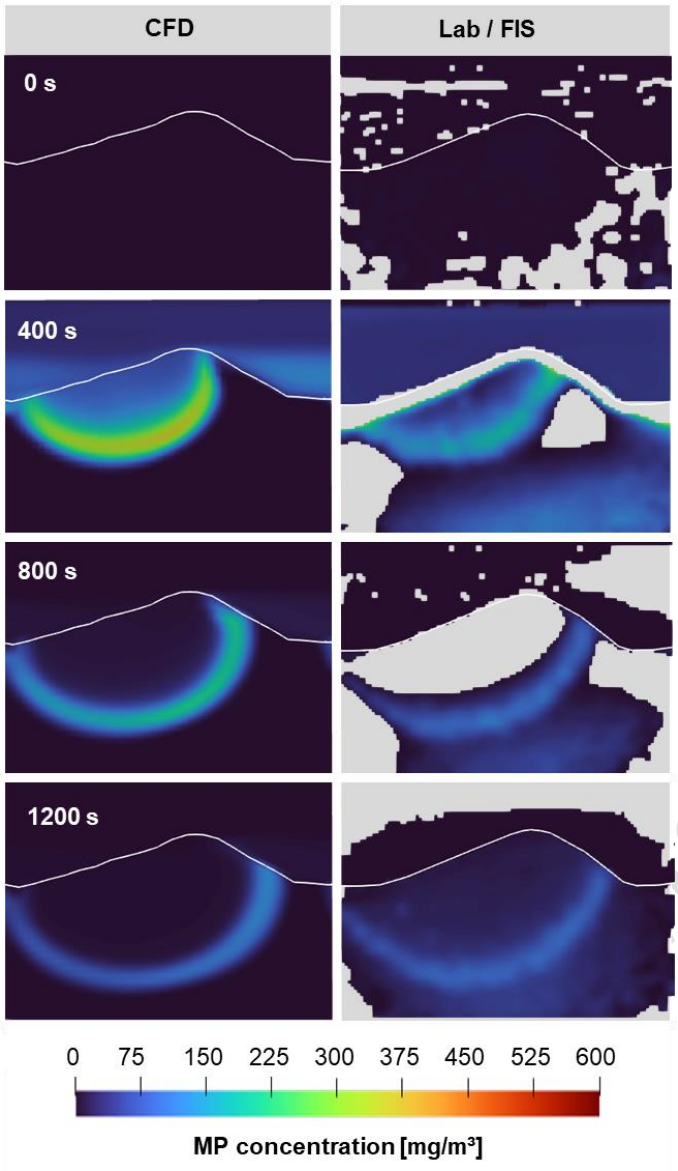

Figure 7. MP infiltration into the reference ripple

To quantitatively assess the propagation speed of the concentration front through the streambed ripple, the concentration over a vertical section at x=3.77 m was extracted from the physical and numerical models (Figure 1B slice sampling bar). To compare the propagation speed, the time when the peak concentration passed through the section at different depths is analyzed in Figure 8. Additionally, for each sampling point the interval of presence of the respective highest 5% of the measured MP concentrations is shown. With an average relative error of 13.1% in the surface water section and 5.3% in the streambed, the exact peak arrival times are predicted satisfactorily by the model. Additionally, the interval, where the largest 5% of the MP concentration passes over the monitoring points has been extracted and shown in the figure. The comparison shows a close match of these intervals between the two datasets, as they coincide for all sampled points. When comparing the mean time of these intervals, the relative error within the surface water section is reduced to 8.3% in the surface water and to 4.7% in the HZ. These intervals furthermore highlight the previously mentioned spatial variability of the infiltration fronts within the porous medium. While the CFD results show a monotonically increasing interval length with depth, the interval width of the lab-measured data is overall increasing with depth, but not monotonically.

Due to the overexposure of the FIS data for the HZ in the boundary layer (blanked areas in Figure 7), the propagation curves had to be reconstructed partially through curve fitting. The parameters are given in the supplementary material S2.

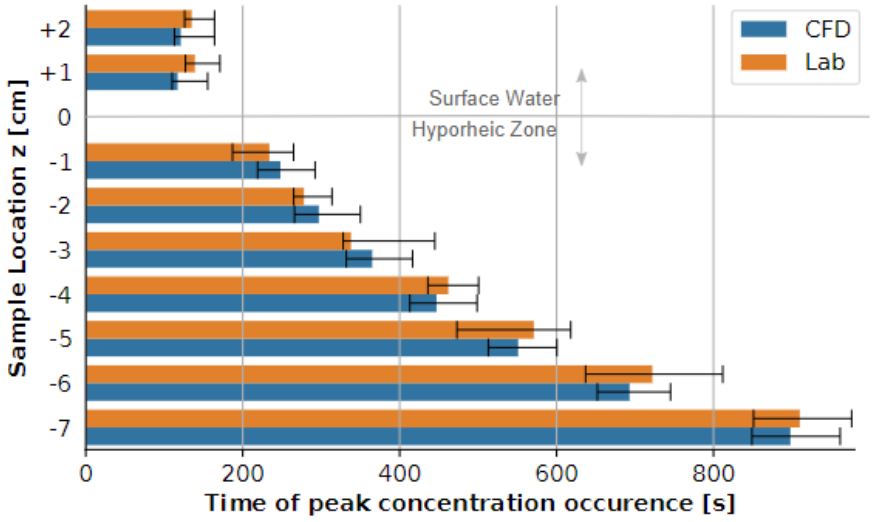

Figure 8. Arrival time of peak concentration at the slice sampling bar below the ripple crest at x = 3.77 m. The interval markers depict the times where 95% of the respective maximum concentration is reached at the respective sampling point.

The quantitative assessment of the MP transport is carried out via comparison between the simulated and observed MP breakthroughs at the up- and downstream ends of the flume as well as within the monitoring window. The concentration peak passes through the experimental section within 75 s. Figure 9 indicates the breakthrough curves resulting from the inflow and outflow concentrations in the

experimental section for the initial 750 s of the experiment. As the in- and outflow concentrations reach the lower quantification limit of the fluorometers (0.36 mg/m³) at around 700 s and 750 s respectively, the mass balance cannot be fully closed based on the fluorometer data. The dataset extracted from the digital twin model is matching the fluorometer data from the laboratory experiment. As the upstream fluorometer serves as the inflow boundary condition for the MP particles in the CFD model, both time series are identical (Figure 9A). The injection starts at t = 40 s. 50 % of the mass is injected before t=144s, and 99 % by t = 430 s. The downstream fluorometer model results correlate closely with the laboratory measurements at a determination coefficient of R^2 = 0.9943 and show a normalized root mean square error (NRMSE) of 0.0148. In regard to the passed mass (i.e. the curve integral of the display concentration curve), 50% of the injected MP mass passed within 199s and 200s for laboratory and model respectively. 90 % of the particle mass passed through the experimental section after 384 s and 367 s respectively. Upon reaching the quantification limit of the lab fluorometers at 750 s, 95.11 % of the injected particles exited the laboratory model, while 98.67 % have been discharged in the CFD model.

With the CFD model, the mass fraction of MP particles in the streambed sediment and surface water compartments can be tracked separately as well as globally without relying only on the in- and outflow measurements. After 504 s, the total particle mass present in the streambed sediments surpassed the one in the surface water compartment. At this point, the fluorometer data indicates that 96.9 % of the MP particles have passed through the laboratory flume, compared to 96.6% obtained from the CFD results data indicates that 96.6 % of the particles have been transported through the digital twin (Figure 9A). Both results indicate that the majority of the particles are transported through the surface water section of the flume. The injection of MP into the model stops at 529 s. With the aforementioned passing time of 75 s, the presence of MP in the surface water after 604 s must predominantly result from releases from the HZ.

Apart from the global quantifications, MP infiltration can be analyzed numerically within the monitoring window. The laboratory measurement of the MP concentration in the HZ is taken through the sidewall of the flume, resulting in the monitoring of a quasi-2D plane due to the opacity of the sediment. For the surface water section, the FIS is also detecting the concentrations behind the HZ monitoring plane, as the water is not blocking the fluorescent signal from the particles. The CFD-equivalent for the surface water section is therefore the average over the complete flume width rather than only the 2D section at the outer wall.

To analyze the MP quantities in the surface flow and the HZ, the monitoring window is reduced to the quantification plane (Figure 1B), which comprises a single ripple without fringe areas, minimizing the areas of lower data quality along the outer edges of the monitoring window (Figure 1). On the quantification plane, the average concentration of MP is calculated for the surface water and HZ over time as shown in Figure 9B. The modeled distribution shows a good match to the laboratory measurements, with a coefficient of determination R^2 = 0.9912. The peak is slightly over-predicted with a relative error of 5.9 %, while the overall NRMSE is at 0.0213.

The data shows that the average concentration in the surface and subsurface are matching between

laboratory and CFD, with the CFD model resulting in slightly reduced (≤ 20 mg/m³) concentrations in the decay period of the subsurface MP concentration. After 550 s runtime, the concentrations in laboratory and CFD model are closely matching.

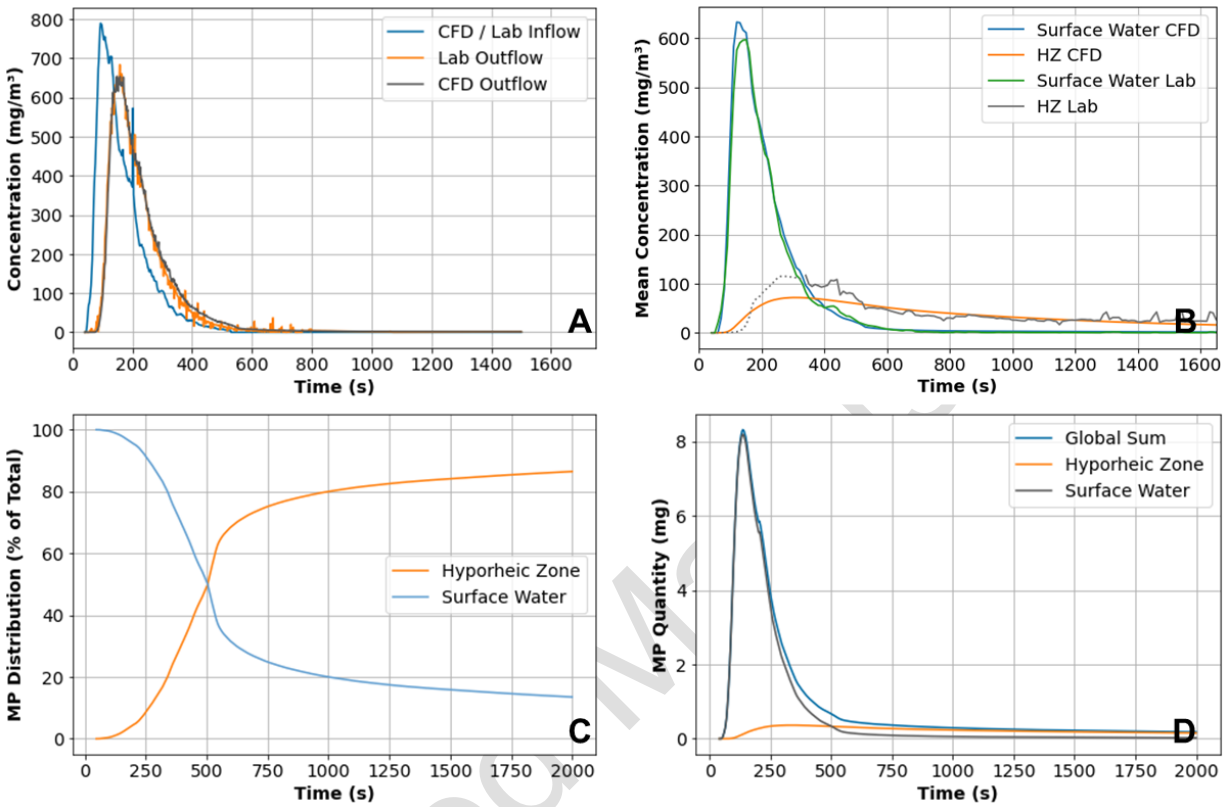

Figure 9. Volumetric MP transport validation in the model: (A) Upstream and downstream MP concentration measurements in the surface flow (B) Average of MP concentration in the quantification plane (dotted line shows extrapolated data) (C) Distribution of MP particles between surface water and HZ (from CFD) (D) Temporal distribution of MP in the model (from CFD)

3.4 Transport of 10 µm MP Particles

Due to physical limitations of the sensor equipment, laboratory comparison data for the 10 µm experiment is only available within the monitoring window. As the physical particle size is close to the size of a sensor pixel, the recording of the quantities is not as reliable as for smaller particles and results in noisier datasets. Despite these limitations, the data can be compared to the simulation data.

While the infiltration patterns as well as the transport flow paths through the HZ are controlled by the hyporheic flow cells as in the case of the smaller 1 µm particles, the propagation speed of the concentration front (the “sickle”) is reduced in comparison to the experiment with 1 µm particles. This is not only noticeable in the qualitative comparison (Figure 10), but also in the comparison of the peak transit times (Figure 11). As the retarded transport is evident, the retardation factor introduced in Equation 2 has been utilized in an attempt to account for this. The retardation factor is used in the transport equation of the HZ only, so that the surface water transport is not retarded.

Comparison of the experimental and simulated peak transit times for 10 µm particles reveals that the use of a single retardation factor can improve model fit either for the upper or the lower segments of the HZ, but not for both at the same time. This indicates that retardation is not steady and increases with flow path length and time. The quantification in the reference plane also reveals that the model overestimates the magnitude of particle infiltration into the HZ for all retardation options (Figure 12), but replicates the particle behavior in the surface water compartment closely.

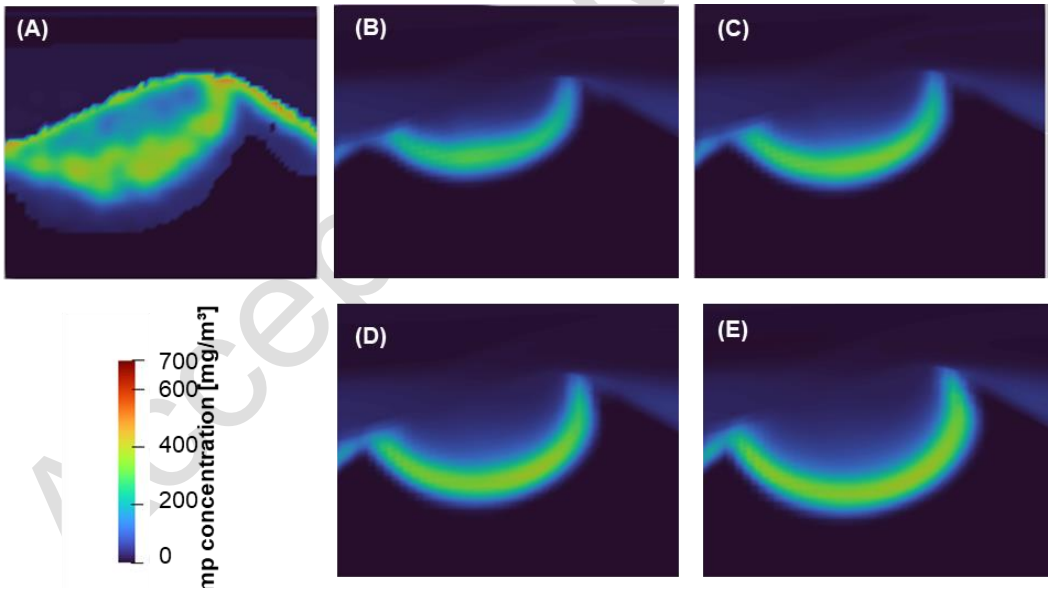

Figure 10. Comparison of infiltration pattern at t = 400 s. Experimental data (A) and simulated patterns for different retardation factors: 5 (B), 4 (C), 2 (D), 1.25 (E).

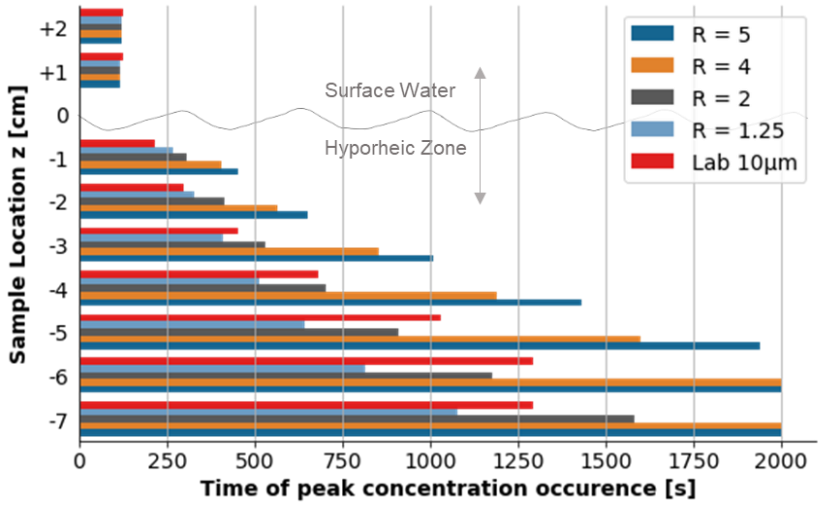

Figure 11. Propagation time of Peak concentration at x = 3.77 m, 10 µm MP particles and CFD runs with different retardation factors.

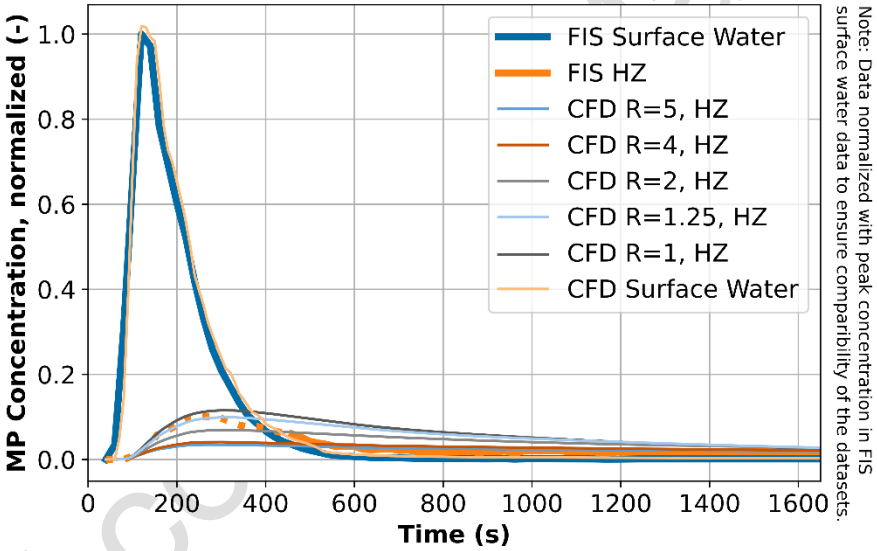

Figure 12. MP concentrations in monitoring section, 10µm PS beads

4 DISCUSSION

4.1 Hydraulic Conditions

The hydraulic conditions in the flume were adequately represented in the CFD model lending credibility to the chosen model setup. The general features of the flow field, as well as the velocity magnitudes computed in the model matched the PIV records closely. Specifically flow conditions close to the streambed interface, where infiltration into the sediment bed occurred, the model provided accurate results. Towards the air-water interface, the model results deviated by up to 0.07 m/s, as the lab-recorded velocity dropped significantly towards the interface. This can be explained by deficiencies of the PIV records towards the surface. The simulation results indicated significant secondary flow in the narrow channel, which was expected given the channel geometry and low water depth. Due to the complex hydraulics of narrow flumes as well as the pronounced ripple structure, high-order turbulence modeling, e.g., using LES, is required to compute the flow conditions in the flume with a sufficient level of detail. Test runs with RANS models also resulted in reduced hyporheic exchange rates, leading to MP concentrations and MP distributions in the HZ that differed significantly from the laboratory results. This suggests that for flume channels, which are commonly narrow relative to the flow depth the hyporheic flow and transport problem might not be adequately approximated with a 2D model and the modeling strategy should be selected with care.

It could be shown that the fully integrated simulation is significantly increasing the accuracy of the modeling results in the present case. The lack of eddy formation in the ripple valleys leads to inaccurate pressure values on the streambed interface in the simulated non-coupled test case with no hyporheic zone. This would result in inaccurate estimates of the hyporheic exchange flux in a weakly (consecutively) coupled model, which would use the independently simulated pressure field over the streambed as the coupling boundary condition for the hyporheic flow model. These differences will be specifically relevant in cases with pronounced bedform structures, where the surface water flow field is strongly influenced by the shape of the ripples and the influence of the underlying bedform on the overall flow field is significant (Zhou and Endreny, 2013).

This is also in line with the findings presented in (Sobhi Gollo et al., 2022b). In this comparative study, a rippled streambed has been modeled using an integrated and a coupled approach. Their investigated case features a slightly different and more conductive streambed geometry and larger flow velocities than in our case. Furthermore, the set of equations used to compute the hydraulic losses in the porous medium differs. The reported qualitative pressure differences over the ripple, with larger differences over the ripple crest and a decline in the valley, as well as the differences in the velocity magnitude are in general agreement with our findings. This is further highlighting the importance of integrated modeling approaches for the investigation of rippled streambeds.

The computation of the flow conditions in the HZ relies on a Darcy-based loss term. The Darcy equation is valid in groundwater flows for laminar flow conditions only, which are present at Reynolds numbers of

up to 300 (Dybbs and Edwards, 1984). In the presented study, Reynolds numbers in the sediments did not exceed the value of 50, placing the flow problem in a laminar flow regime and the Darcy loss term has shown to produce an accurate flow field. If coarser sediments were to be used, which may facilitate more prominent non-laminar flows in the uppermost sediment layers, additional validation experiments would be needed to confirm the applicability of the utilized equations, or to calibrate additional Forchheimer or other loss coefficients as for example presented in (Broecker et al., 2019).

4.2 MP Particle Transport

Simulation results indicate that the transport of the 1 µm MP particles in a sandy HZ can reasonably be modeled using the advection-dispersion equation in a fully integrated hydrodynamic model (i.e. flow in the open water and sediments is solved with one set of equations simultaneously) that accurately accounts for the hydrodynamic feedbacks and exchange flows between the open water and hyporheic domains. The model could adequately reproduce the shape and temporal evolution of the particle concentration fronts in the HZ (Figure 7) and the experimental breakthrough curves for 1 µm MP particles in the open water and in the sediment were matched very well (Figure 9). The trajectory of the particle peak concentrations with depth in the HZ could also be captured well (Figure 8). Due to the limitations of the MP detection in the laboratory, the concentration fields obtained from the CFD simulations are more refined, showing a more sharply defined spatial extent than the results obtained from the laboratory (Figure 8). The quantitative comparison of the results shows nonetheless that the model is accurately predicting the transport quantities and locations (Figure 9). The deviations between observed and simulated MP concentrations in the HZ between 400-500 s, as shown in Figure 9B fall within the period where the MP transport is still predominantly located within the surface water compartment and are related to large areas in the detection window with non-plausible concentrations, which were present in the FIS records during this period. However, the overall MP outflow record at the downstream end of the experimental stretch was closely matched by the model, indicating that the temporary deviation between experiment and model can be attributed to detection artefacts.

It cannot be ruled out that in the experiment single particles were trapped in the pore spaces and bound to the surrounding mineral particles, e.g. by electrochemical bonds (Lu et al., 2021). Also, physical retention of individual particles in the pore space is theoretically possible, but our observed and simulated breakthrough curves suggest that there is no significant retention of the 1 µm particles in the sediments and that they appear to move through the HZ more or less uninhibited like a non-adsorbing, conservative solute. As single particles of 1 µm size are not detectable in the sediments with the utilized online methods, we could not further corroborate this statement experimentally. However, this finding is backed by the results reported in (Goeppert and Goldscheider, 2021), who showed similar, unretarded transport of small, similar size MP particles (1, 2 and 5 µm) in a sandy alluvial aquifer.

In contrast, for larger particles, our results suggest that retention processes will play a more crucial role. We attribute the delayed transport of the 10 µm particles through the HZ to temporary retention of the particles in the sediments as they, due to their size, cannot move as smoothly through the pore spaces as the 1 µm particles. As shown in Figure 12, the infiltration quantity of 10 µm compared to the 1 µm

particles is reduced, with the concentration in the HZ being approximately halved. This also highlights the requirement of a differentiated treatment of the different MP size ranges in transport modeling.

The comparison case with 10 µm MP particles reveals the limitations of the presented approach for larger MP particles. While the surface water transport is modeled accurately, the infiltration into the HZ is overestimated, particularly during the later phase of the experiment, and the general transport pattern is not matched accurately (Figure 12). The particle propagation within the HZ is furthermore delayed (Figure 10, 11). Our analyses showed that the retardation factor required to compensate for the mismatch between laboratory observation and modeling results is increasing with depth, suggesting that the particles are getting increasingly retarded with growing flow path length. This transport behavior with non-steady retardation cannot easily be implemented in the Eulerian approach used here and may require the use of an adapted Lagrangian particle tracking approach. Furthermore, the presented experimental approach needs to be refined to deliver accurate validation data for more complex numerical setups, e.g. by employing optical particle tracking within the FIS.

4.3 Limitations and future challenges

As (Dong et al., 2022) have shown, the transport behavior of MP particles in partly and fully saturated porous media also depends on the polymer type and the biogeochemical conditions of the surrounding medium. Such effects could not be fully addressed in this study. To test a broader, more general applicability of our modeling approach, additional experiments with different particles and under different biogeochemical regimes in the sediments need to be carried out. However, the market availability of suitable particles is a limiting factor for the laboratory work, as only a relatively small range of polymer types and particle shapes is available with the required fluorescent properties.

Given experimental limitations, studies usually work with high non-realistic MP concentrations, which are significantly higher compared to what is usually observed in streams. To what degree this affects the transfer of experimental results to natural systems remains to be tested in future work.

Using opaque sediment, the MP concentrations can only be monitored along the glass interface of the flume, if the hyporheic continuum should not be disturbed. To our knowledge, there are also no suitable methods to continuously monitor MP concentrations within 2D sections in sediment bodies. Hence, only singular measurements after the experimental runs could be taken either by extracting sediment cores and analyzing them manually or by using more involved non-destructive methods (Tötzke et al., 2021). This approach will, however, not yield information on the infiltration dynamics and is therefore not suited to improve our mechanistic understanding of MP transport. This leads to uncertainties regarding MP transport in the HZ away from the flume wall. However, the accurate representation of the hydraulic conditions in the flume and of the transport in the surface water and in the sediment along the sidewalls in the 3D digital twin model, suggest that the concentrations simulated in the digital twin are in fact a good representation of the actual transport of MP particles in the laboratory flume experiment.

Our results show that the transport and infiltration behavior of particles of 1 µm and 10 µm varies within

the same sediment type. We hypothesized that the behavior is dependent on the relation between pore and particle size, but additional experimental investigations are needed to further corroborate this. Furthermore, the effects of different biogeochemical regimes in sediments on particle transport within the HZ are not considered in our study and should be addressed in future work.

Long-term retention cannot be adequately analyzed with the modeling approach or the laboratory setup. The spatial averaging method employed for the laboratory data does not allow detecting single particles within the sediments. Therefore, the retention by processes such as heteroaggregation of MP with mineral particles, or physical retention in the pore space, e.g. by size-exclusion, cannot be detected and therefore also not be reliably implemented in the used numerical model at this stage. Here pore-scale models would be needed.

4.4 Specific utility of the digital twin model

In the previous paragraph we discussed some of the limitations of the experimental design with regard to a seamless detection of MP concentrations throughout the flume system. The calibrated digital twin model of the flume experiment can overcome some of the limitations of the laboratory experiment, at least for the small particles. The successful calibration of the model to the hydraulics in the flume as well as to the propagation of MP concentration fronts at the sidewalls of the flume, lends credibility to the consistency of the model in terms of an accurate representation of the true 3D flows in the HZ in the flume. While in the flume experiment hyporheic MP concentrations can only be measured and monitored through the sidewall of the flume, i.e. at the outer boundary of the flow field, the numerical approach allows the user to look inside the porous continuum and investigate the flow and transport patterns in all three dimensions. Furthermore, the numerical model resolves the flow over the entire domain, so that the analyses are not limited to a fixed monitoring window resulting from limited viewing angles of monitoring equipment. All physical parameters can be directly derived from the CFD output data, while in the laboratory flume, each parameter (set) requires specific instrumentation. Physical limitations, such as the size of the laboratory, the limited ability to recirculate particle-laden flows or detection limits can be overcome with the numerical model. Also, the implementation of scenarios is easily facilitated with a numerical model, as materials and geometries can be changed efficiently digitally and different virtual particles would not require different monitoring setups as long as they generally adhere to the same general transport mechanisms identified for the original particles.

However, to produce reliable results, a numerical model has to be validated, which is usually done through laboratory experiments. Hydraulic conditions can be reliably predicted by standalone numerical models, as they have been studied extensively. In the relatively new and evolving field of MP transport in fluvial systems, however, the governing transport processes are still poorly understood and subject to current research. Therefore, reliable transport modeling of MP in fluvial systems needs to be backed up by physical studies confirming the applied transport models**.** In any case, an integral numerical model can be used to explore hydraulic effects for a given flume or field site geometry to inform an appropriate study design.

As the online particle detection is currently limited to a quasi-2D section at the flume wall, the overall width of the flume is not relevant for the laboratory measurements beyond the general hydraulic conditions. The narrow flume also is reducing the amount of MP particles required to generate detectable MP concentrations in the monitoring window. To this end, the narrow flume presents an efficient way of carrying out the validation experiments for the digital twin.

In comparison, more conceptual, stochastic approaches, such as the model utilized in (Drummond et al., 2020), can usually represent mass balances well at larger scales. However, local effects, such as more complex hydrodynamic conditions or specific infiltration behavior of differently sized particles can only indirectly be implemented in those more aggregated approaches. The presented integral, mechanistic modeling approach in turn allows us to analyze the spatiotemporal transport behavior in more detail, which could inform parameterizations in simpler models. It is thus complementing the conceptual modeling

approaches towards the smaller scales, which provides additional insights, e.g. with respect to the spatiotemporal particle distributions or transit times. This is required not only for a deeper mechanistic understanding of MP pollution in fluvial systems, but can also provide feedback to the larger-scale approaches to improve the overall modeling accuracy.

5 SUMMARY AND CONCLUSIONS

In this study we could show that the investigated 1 µm MP particles are transported through the hyporheic zone like a solute tracer. Our simulations indicate that the majority (96.6%) of the MP particle pulse is transported in the surface water section and only a very small fraction (3.4%) infiltrates into the HZ. Within the HZ the concentration peak of the 1 µm particles is following the advective transport of the water as it has been shown for solute transport in the HZ (Broecker et al., 2021). For larger particles, such as the investigated 10 µm PS particles, the physical and numerical investigations show that particle transport is delayed in comparison to the 1 µm particles. We attributed this to additional physicochemical processes, which cannot be mechanistically elucidated with the experimental and modeling setups in this study. Instead we proposed and tested an effective description using a constant retardation factor as commonly used to describe retardation of solutes undergoing adsorption and desorption. While a constant retardation factor could not account for the delays of the particle breakthroughs at all depths, formulations with a time-variant retardation factor, which increases with flow path length, are theoretically conceivable, but would require a Lagrangian modeling approach.

In a conceptual modeling study (Drummond et al., 2020) concluded that MP particles, ranging in size from 1 – 100 µm, are advectively transported through the HZ with around half of the particles being retained temporarily. Our findings suggest that the transport of larger particles (10 µm) through the HZ is retarded indicating a temporary retention. While the investigated 1 µm particles appear to be transported in the investigated system like a conservative, non-adsorbing, solute tracer, retardation effects are detected for the larger particles. Using a constant retardation factor the match between observed and modeled breakthrough of the concentration peak at different depth could be improved, but not at the same rate over the entire depth range. For a good match at shallower depth retardation at deeper depth was underestimated while a good match at deeper depth was accompanied with an overestimation of retardation at shallow depth. This suggests that retardation may increase with flow path length, illustrating that further investigations are required to improve our mechanistic understanding of the dominant transport processes for MP particles within the size range of 1 – 100 µm in the pore space of hyporheic sediments. As our study is closely focusing on small-scale effects in the transport of MP particles in the HZ, the differences in transport behavior between seemingly similar MP particles will be more apparent (and relevant), than in coarser, larger-scale models, which represent a diverse particle mixture with a wide variability of size, density and polymer types as a particle distribution. The modeling approach proposed here, which uses scalar transport equations to model MP transport in the HZ might therefore be a viable and practical complement to the simpler, coarser models, to simulate spatial infiltration patterns, as successfully demonstrated in this study.

The application of a fully integrated digital twin model revealed the peculiarities of the laboratory flume experiment and could further provide new insights into potential limitations of commonly used coupled, numerical modeling approaches. The results show that both the narrow laboratory flume as well as the CFD model produce valid results for MP transport investigations in and into the HZ, but effects such as

secondary currents or hydraulic feedbacks from the HZ to the surface water have to be individually assessed and considered.

To our knowledge, the presented approach for mechanistic modeling of integral open-water and hyporheic flow and transport of MP is the first to be explicitly validated against experimental (flume) data not only in terms of qualitative observations of concentration patterns, but also in terms of the quantification of fluxes. The very good agreement between the model and the observational data suggests that the hydraulic conditions and the transport behavior for 1 µm MP particles are accurately replicated by the model. This makes the presented modeling approach not only amenable to analyses of small MP particle transport in the HZ, but with additional validation also to other research questions involving hyporheic exchange flows and transport processes. Our results further suggest that the retardation of larger 10 µm particles could be accounted for using a dynamic retardation factor. Additional processes acting on even larger particles, causing further retardation or even permanent retention in the sediments, need to be investigated in future pore-scale studies.

6 AUTHOR CONTRIBUTION STATEMENT

FD co-developed the research idea, developed the numerical modeling setup, assisted with the flume experiment setup, carried out the numerical modeling and validation, processed, analyzed and interpreted the numerical and laboratory datasets, and wrote the initial draft of the manuscript. JPB developed the laboratory setup and carried out the flume experiment, processed the experimental dataset and assisted in the data interpretation. PA assisted in data interpretation. SF supported the laboratory experiments. JHF conceived the project, co-developed the research idea, and assisted in the data interpretation. All authors contributed to reviewing and editing the manuscript.

7 ACKNOWLEDGEMENT

This study was funded by the Deutsche Forschungsgemeinschaft (DFG, German Research Foundation) – Project Number 391977956 – SFB 1357. Additional funding was provided by the Helmholtz-Centre for Environmental Research (Topic 5, subtopic 5.2).

8 REFERENCES

Ahmadi, P., Elagami, H., Dichgans, F., Schmidt, C., Gilfedder, B.S., Frei, S., Peiffer, S., Fleckenstein, J.H., 2022. Systematic Evaluation of Physical Parameters Affecting the Terminal Settling Velocity of Microplastic Particles in Lakes Using CFD. Front. Environ. Sci. 10, 875220. https://doi.org/10.3389/fenvs.2022.875220

Amoatey, P., Baawain, M.S., 2019. Effects of pollution on freshwater aquatic organisms. Water Environment Research 91, 1272–1287. https://doi.org/10.1002/wer.1221

Andrady, A.L., 2011. Microplastics in the marine environment. Marine Pollution Bulletin 62, 1596–1605. https://doi.org/10.1016/j.marpolbul.2011.05.030

Besseling, E., Foekema, E.M., van den Heuvel-Greve, M.J., Koelmans, A.A., 2017a. The Effect of Microplastic on the Uptake of Chemicals by the Lugworm *Arenicola marina* (L.) under Environmentally Relevant Exposure Conditions. Environ. Sci. Technol. 51, 8795–8804. https://doi.org/10.1021/acs.est.7b02286

Besseling, E., Quik, J.T.K., Sun, M., Koelmans, A.A., 2017b. Fate of nano- and microplastic in freshwater systems: A modeling study. Environmental pollution (Barking, Essex : 1987) 220, 540–548. https://doi.org/10.1016/j.envpol.2016.10.001

Boos, J., Gilfedder, B.S., Frei, S., 2021. Tracking Microplastics Across the Streambed Interface: Using Laser-Induced-Fluorescence to Quantitatively Analyze Microplastic Transport in an Experimental Flume. Water Resources Research 57. https://doi.org/10.1029/2021WR031064

Boos, J.-P., Dichgans, F., Gilfedder, B.-S., Frei, S., 2022. An Experimental Method to Quantitatively Assess the Transport of Microplastic Particles in Fluvial Systems, in: Proceedings of the 39th IAHR World Congress. Presented at the 39th IAHR World Congress From Snow to Sea, International Association for Hydro-Environment Engineering and Research (IAHR), pp. 5030–5034. https://doi.org/10.3850/IAHR-39WC252171192022487

Broecker, T., Elsesser, W., Teuber, K., Özgen, I., Nützmann, G., Hinkelmann, R., 2018. High-resolution simulation of free-surface flow and tracer retention over streambeds with ripples. Limnologica 68, 46–58. https://doi.org/10.1016/j.limno.2017.06.005

Broecker, T., Sobhi Gollo, V., Fox, A., Lewandowski, J., Nützmann, G., Arnon, S., Hinkelmann, R., 2021. High-Resolution Integrated Transport Model for Studying Surface Water–Groundwater Interaction. Groundwater 59, 488–502. https://doi.org/10.1111/gwat.13071

Broecker, T., Teuber, K., Sobhi Gollo, V., Nützmann, G., Lewandowski, J., Hinkelmann, R., 2019. Integral Flow Modelling Approach for Surface Water-Groundwater Interactions along a Rippled Streambed. Water 11, 1517. https://doi.org/10.3390/w11071517

Burns, E.E., Boxall, A.B.A., 2018. Microplastics in the aquatic environment: Evidence for or against adverse impacts and major knowledge gaps: Microplastics in the environment. Environ Toxicol Chem 37, 2776–2796. https://doi.org/10.1002/etc.4268

Castañeda, R.A., Avlijas, S., Simard, M.A., Ricciardi, A., 2014. Microplastic pollution in St. Lawrence River sediments. Can. J. Fish. Aquat. Sci. 71, 1767–1771. https://doi.org/10.1139/cjfas-2014-0281

Choi, J.S., Kim, K., Hong, S.H., Park, K.-I., Park, J.-W., 2021. Impact of polyethylene terephthalate microfiber length on cellular responses in the Mediterranean mussel Mytilus galloprovincialis. Marine Environmental Research 168, 105320. https://doi.org/10.1016/j.marenvres.2021.105320

Constant, M., Alary, C., De Waele, I., Dumoulin, D., Breton, N., Billon, G., 2021. To What Extent Can Micro- and Macroplastics Be Trapped in Sedimentary Particles? A Case Study Investigating Dredged Sediments. Environ. Sci. Technol. 55, 5898–5905. https://doi.org/10.1021/acs.est.0c08386

Cook, S., Chan, H.-L., Abolfathi, S., Bending, G.D., Schäfer, H., Pearson, J.M., 2020. Longitudinal dispersion of microplastics in aquatic flows using fluorometric techniques. Water Research 170, 115337. https://doi.org/10.1016/j.watres.2019.115337

D'Avignon, G., Gregory-Eaves, I., Ricciardi, A., 2022. Microplastics in lakes and rivers: an issue of emerging significance to limnology. Environ. Rev. 30, 228–244. https://doi.org/10.1139/er-2021-0048

Domercq, P., Praetorius, A., MacLeod, M., 2022. The Full Multi: An open-source framework for modelling the transport and fate of nano- and microplastics in aquatic systems. Environmental Modelling & Software 148, 105291. https://doi.org/10.1016/j.envsoft.2021.105291

Dong, S., Zhou, M., Su, X., Xia, J., Wang, L., Wu, H., Suakollie, E.B., Wang, D., 2022. Transport and retention patterns of fragmental microplastics in saturated and unsaturated porous media: A real-time pore-scale visualization. Water Research 214, 118195.

https://doi.org/10.1016/j.watres.2022.118195
Drummond, J.D., Nel, H.A., Packman, A.I., Krause, S., 2020. Significance of Hyporheic Exchange for Predicting Microplastic Fate in Rivers. Environ. Sci. Technol. Lett. 7, 727–732. https://doi.org/10.1021/acs.estlett.0c00595
Drummond, J.D., Schneidewind, U., Li, A., Hoellein, T.J., Krause, S., Packman, A.I., 2022. Microplastic accumulation in riverbed sediment via hyporheic exchange from headwaters to mainstems. Sci. Adv. 8, eabi9305. https://doi.org/10.1126/sciadv.abi9305
Dudunake, T., Tonina, D., Reeder, W.J., Monsalve, A., 2020. Local and Reach-Scale Hyporheic Flow Response From Boulder-Induced Geomorphic Changes. Water Resour. Res. 56. https://doi.org/10.1029/2020WR027719
Dybbs, A., Edwards, R.V., 1984. A New Look at Porous Media Fluid Mechanics — Darcy to Turbulent, in: Bear, J., Corapcioglu, M.Y. (Eds.), Fundamentals of Transport Phenomena in Porous Media. Springer Netherlands, Dordrecht, pp. 199–256. https://doi.org/10.1007/978-94-009-6175-3_4
Elliott, A.H., Brooks, N.H., 1997. Transfer of nonsorbing solutes to a streambed with bed forms: Laboratory experiments. Water Resour. Res. 33, 137–151. https://doi.org/10.1029/96WR02783
Ferziger, J.H., Perić, M., Street, R.L., 2020. Computational Methods for Fluid Dynamics. Springer International Publishing, Cham. https://doi.org/10.1007/978-3-319-99693-6
Frei, S., Piehl, S., Gilfedder, B.S., Löder, M.G.J., Krutzke, J., Wilhelm, L., Laforsch, C., 2019. Occurence of microplastics in the hyporheic zone of rivers. Scientific reports 9, 15256. https://doi.org/10.1038/s41598-019-51741-5
Frias, J.P.G.L., Nash, R., 2019. Microplastics: Finding a consensus on the definition. Marine Pollution Bulletin 138, 145–147. https://doi.org/10.1016/j.marpolbul.2018.11.022
Goeppert, N., Goldscheider, N., 2021. Experimental field evidence for transport of microplastic tracers over large distances in an alluvial aquifer. Journal of Hazardous Materials 408, 124844. https://doi.org/10.1016/j.jhazmat.2020.124844
Haque, M.I., Mahmood, K., 1985. Geometry of Ripples and Dunes. Journal of Hydraulic Engineering 111, 48–63. https://doi.org/10.1061/(ASCE)0733-9429(1985)111:1(48)
Harvey, J.W., Bencala, K.E., 1993. The Effect of streambed topography on surface-subsurface water exchange in mountain catchments. Water Resour. Res. 29, 89–98. https://doi.org/10.1029/92WR01960
Hirt, C.W., Nichols, B.D., 1981. Volume of fluid (VOF) method for the dynamics of free boundaries. Journal of Computational Physics 39, 201–225. https://doi.org/10.1016/0021-9991(81)90145-5
Hoellein, T.J., Shogren, A.J., Tank, J.L., Risteca, P., Kelly, J.J., 2019. Microplastic deposition velocity in streams follows patterns for naturally occurring allochthonous particles. Scientific reports 9, 3740. https://doi.org/10.1038/s41598-019-40126-3
Horton, A.A., Dixon, S.J., 2018. Microplastics: An introduction to environmental transport processes. WIREs Water 5. https://doi.org/10.1002/wat2.1268
Janssen, F., Cardenas, M.B., Sawyer, A.H., Dammrich, T., Krietsch, J., de Beer, D., 2012. A comparative experimental and multiphysics computational fluid dynamics study of coupled surface-subsurface flow in bed forms. Water Resour. Res. 48. https://doi.org/10.1029/2012WR011982
Jing, S., Yang, W., Chen, Y., 2019. Smooth Open Channel with Increasing Aspect Ratio: Influence on Secondary Flow. Water 11, 1872. https://doi.org/10.3390/w11091872
Kirstein, I.V., Kirmizi, S., Wichels, A., Garin-Fernandez, A., Erler, R., Löder, M., Gerdts, G., 2016. Dangerous hitchhikers? Evidence for potentially pathogenic Vibrio spp. on microplastic particles. Marine Environmental Research 120, 1–8. https://doi.org/10.1016/j.marenvres.2016.07.004
Koelmans, A.A., Gouin, T., Thompson, R., Wallace, N., Arthur, C., 2014. Plastics in the marine environment. Environ Toxicol Chem 33, 5–10. https://doi.org/10.1002/etc.2426
Laermanns, H., Reifferscheid, G., Kruse, J., Földi, C., Dierkes, G., Schaefer, D., Scherer, C., Bogner, C., Stock, F., 2021. Microplastic in Water and Sediments at the Confluence of the Elbe and Mulde Rivers in Germany. Front. Environ. Sci. 9, 794895. https://doi.org/10.3389/fenvs.2021.794895
Laforsch, C., Ramsperger, A.F.R.M., Mondellini, S., Galloway, T.S., 2021. Microplastics: A Novel Suite of Environmental Contaminants but Present for Decades, in: Reichl, F.-X., Schwenk, M. (Eds.), Regulatory Toxicology. Springer Berlin Heidelberg, Berlin, Heidelberg, pp. 1–26. https://doi.org/10.1007/978-3-642-36206-4_138-1
Lebreton, L.C.M., van der Zwet, J., Damsteeg, J.-W., Slat, B., Andrady, A., Reisser, J., 2017. River plastic emissions to the world's oceans. Nat Commun 8, 15611. https://doi.org/10.1038/ncomms15611
Lewandowski, J., Arnon, S., Banks, E., Batelaan, O., Betterle, A., Broecker, T., Coll, C., Drummond, J., Gaona Garcia, J., Galloway, J., Gomez-Velez, J., Grabowski, R., Herzog, S., Hinkelmann, R., Höhne, A., Hollender, J., Horn, M., Jaeger, A., Krause, S., Löchner Prats, A., Magliozzi, C., Meinikmann, K., Mojarrad, B., Mueller, B., Peralta-Maraver, I., Popp, A., Posselt, M., Putschew,

A., Radke, M., Raza, M., Riml, J., Robertson, A., Rutere, C., Schaper, J., Schirmer, M., Schulz, H., Shanafield, M., Singh, T., Ward, A., Wolke, P., Wörman, A., Wu, L., 2019. Is the Hyporheic Zone Relevant beyond the Scientific Community? Water 11, 2230. https://doi.org/10.3390/w11112230

Li, B., Liu, X., Kaufman, M.H., Turetcaia, A., Chen, X., Cardenas, M.B., 2020. Flexible and Modular Simultaneous Modeling of Flow and Reactive Transport in Rivers and Hyporheic Zones. Water Resour. Res. 56. https://doi.org/10.1029/2019WR026528

Lu, T., Gilfedder, B.S., Peng, H., Peiffer, S., Papastavrou, G., Ottermann, K., Frei, S., 2021. Relevance of Iron Oxyhydroxide and Pore Water Chemistry on the Mobility of Nanoplastic Particles in Water-Saturated Porous Media Environments. Water Air Soil Pollut 232, 168. https://doi.org/10.1007/s11270-021-05125-z

Mani, T., Hauk, A., Walter, U., Burkhardt-Holm, P., 2016. Microplastics profile along the Rhine River. Sci Rep 5, 17988. https://doi.org/10.1038/srep17988

Mani, T., Primpke, S., Lorenz, C., Gerdts, G., Burkhardt-Holm, P., 2019. Microplastic Pollution in Benthic Midstream Sediments of the Rhine River. Environ. Sci. Technol. 53, 6053–6062. https://doi.org/10.1021/acs.est.9b01363

McCormick, A., Hoellein, T.J., Mason, S.A., Schluep, J., Kelly, J.J., 2014. Microplastic is an Abundant and Distinct Microbial Habitat in an Urban River. Environ. Sci. Technol. 48, 11863–11871. https://doi.org/10.1021/es503610r

Meijer, L.J.J., van Emmerik, T., van der Ent, R., Schmidt, C., Lebreton, L., 2021. More than 1000 rivers account for 80% of global riverine plastic emissions into the ocean. Sci. Adv. 7, eaaz5803. https://doi.org/10.1126/sciadv.aaz5803

Napper, I.E., Thompson, R.C., 2020. Plastic Debris in the Marine Environment: History and Future Challenges. Global Challenges 4, 1900081. https://doi.org/10.1002/gch2.201900081

Nikitin, N.V., Popelenskaya, N.V., Stroh, A., 2021. Prandtl's Secondary Flows of the Second Kind. Problems of Description, Prediction, and Simulation. Fluid Dyn 56, 513–538. https://doi.org/10.1134/S0015462821040091

Nizzetto, L., Bussi, G., Futter, M.N., Butterfield, D., Whitehead, P.G., 2016. A theoretical assessment of microplastic transport in river catchments and their retention by soils and river sediments. Environ. Sci.: Processes Impacts 18, 1050–1059. https://doi.org/10.1039/C6EM00206D

Petersen, F., Hubbart, J.A., 2021. The occurrence and transport of microplastics: The state of the science. Science of The Total Environment 758, 143936. https://doi.org/10.1016/j.scitotenv.2020.143936

Ren, J., Zhao, B., 2020. Model-Based Analysis of the Effects of Rippled Bed Morphologies on Hyporheic Exchange. J. Hydrol. Eng. 25, 04020023. https://doi.org/10.1061/(ASCE)HE.1943-5584.0001931

Schmidt, C., Krauth, T., Wagner, S., 2017. Export of Plastic Debris by Rivers into the Sea. Environmental science & technology 51, 12246–12253. https://doi.org/10.1021/acs.est.7b02368

Schrank, I., Trotter, B., Dummert, J., Scholz-Böttcher, B.M., Löder, M.G.J., Laforsch, C., 2019. Effects of microplastic particles and leaching additive on the life history and morphology of Daphnia magna. Environmental Pollution 255, 113233. https://doi.org/10.1016/j.envpol.2019.113233

Siegfried, M., Koelmans, A.A., Besseling, E., Kroeze, C., 2017. Export of microplastics from land to sea. A modelling approach. Water research 127, 249–257. https://doi.org/10.1016/j.watres.2017.10.011

Sobhi Gollo, V., Broecker, T., Lewandowski, J., Nützmann, G., Hinkelmann, R., 2022a. Flow and Transport Modeling in Heterogeneous Sediments Using an Integral Approach. Groundwater gwat.13275. https://doi.org/10.1111/gwat.13275

Sobhi Gollo, V., Broecker, T., Lewandowski, J., Nützmann, G., Hinkelmann, R., 2021. An integral approach to simulate three-dimensional flow in and around a ventilated U-shaped chironomid dwelled burrow. Journal of Ecohydraulics 1–11. https://doi.org/10.1080/24705357.2021.1938258

Sobhi Gollo, V., Broecker, T., Marx, C., Lewandowski, J., Nützmann, G., Hinkelmann, R., 2022b. A comparative study of integral and coupled approaches for modeling hydraulic exchange processes across a rippled streambed. Int J Geomath 13, 16. https://doi.org/10.1007/s13137-022-00206-5

Stride, B., Abolfathi, S., Merenchi Galappaththige, N.O., Bending, G., Pearson, J., 2022. Modelling microplastic and solute dispersion in fluvial environments. https://doi.org/10.1002/essoar.10512433.1

Thompson, R.C., Olsen, Y., Mitchell, R.P., Davis, A., Rowland, S.J., John, A.W.G., McGonigle, D., Russell, A.E., 2004. Lost at Sea: Where Is All the Plastic? Science 304, 838–838. https://doi.org/10.1126/science.1094559

Tötzke, C., Oswald, S.E., Hilger, A., Kardjilov, N., 2021. Non-invasive detection and localization of microplastic particles in a sandy sediment by complementary neutron and X-ray tomography. J

Soils Sediments 21, 1476–1487. https://doi.org/10.1007/s11368-021-02882-6
Trauth, N., Schmidt, C., Maier, U., Vieweg, M., Fleckenstein, J.H., 2013. Coupled 3-D stream flow and hyporheic flow model under varying stream and ambient groundwater flow conditions in a pool-riffle system. Water Resour. Res. 49, 5834–5850. https://doi.org/10.1002/wrcr.20442
von Moos, N., Burkhardt-Holm, P., Köhler, A., 2012. Uptake and Effects of Microplastics on Cells and Tissue of the Blue Mussel *Mytilus edulis* L. after an Experimental Exposure. Environ. Sci. Technol. 46, 11327–11335. https://doi.org/10.1021/es302332w
Waldschläger, K., Schüttrumpf, H., 2020. Infiltration Behavior of Microplastic Particles with Different Densities, Sizes, and Shapes—From Glass Spheres to Natural Sediments. Environ. Sci. Technol. acs.est.0c01722. https://doi.org/10.1021/acs.est.0c01722
Weller, H.G., Tabor, G., Jasak, H., Fureby, C., 1998. A tensorial approach to computational continuum mechanics using object-oriented techniques. Comput. Phys. 12, 620. https://doi.org/10.1063/1.168744
Windsor, F.M., Tilley, R.M., Tyler, C.R., Ormerod, S.J., 2019. Microplastic ingestion by riverine macroinvertebrates. Science of The Total Environment 646, 68–74. https://doi.org/10.1016/j.scitotenv.2018.07.271
Xiao, Y., Liu, Jiaming, Wang, N., Gualtieri, C., Zhang, T., Liu, Jieqing, Fu, J., Zhou, J., 2022. Numerical simulation of overbank hyporheic transport and biogeochemical reactions in a compound channel. Hydrological Processes 36. https://doi.org/10.1002/hyp.14670
Yang, S.-Q., Tan, S.K., Wang, X.-K., 2012. Mechanism of secondary currents in open channel flows: SECONDARY CURRENTS, SAND RIDGES, FLOWS. J. Geophys. Res. 117, n/a-n/a. https://doi.org/10.1029/2012JF002510
Zhou, T., Endreny, T.A., 2013. Reshaping of the hyporheic zone beneath river restoration structures. Water Resour. Res. 49, 5009–5020. https://doi.org/10.1002/wrcr.20384